Materials Advances

ROYAL SOCIETY OF CHEMISTRY

PAPER

View Article Online
View Journal | View Issue

Cite this: *Mater. Adv.*, 2026, 7, 1805

Surface-induced alignment of liquid crystal elastomers on commercial polyimide-based films

Elaheh Asgari, *[a] Alexandre Robichaud,[b] Paul-Vahé Cicek[c] and Andy Shih[a]

Liquid crystal elastomers (LCEs) are versatile materials capable of reversible, large-scale deformations in response to external stimuli. The orientation of the liquid crystal mesogens within the polymer network significantly impacts their performance in various applications, including soft robotics and actuators. Here, we present a simple, cost-effective surface-induced alignment technique using off-the-shelf, commercially available Kapton HN films, which—unlike previously reported custom polyimide coatings—inherently possess surface features capable of inducing mesogen alignment and can also be mechanically rubbed to enhance the density and uniformity of surface nanogrooves. This enables the fabrication of monodomain LCE films with controlled alignment through a straightforward mechanical rubbing process, representing a significant advancement in accessibility and scalability compared to prior methods. Atomic force microscopy (AFM) reveals that surface rubbing alters the topography of Kapton films, with rubbing in different directions resulting in distinct roughness profiles. Polarized optical microscopy (POM) analysis of LCE films aligned using this technique demonstrates that rubbing Kapton horizontally or vertically leads to varying degrees of mesogen alignment, with horizontal rubbing producing the highest alignment quality. Thermal actuation tests confirm that the alignment configuration significantly influences the LCE's actuation response, with the planar-aligned films exhibiting uniaxial contraction and twisted-aligned films demonstrating bending behavior due to through-thickness strain mismatch. This mechanistic correlation between surface morphology, mesogen orientation, and actuation behavior offers new insights into alignment-driven deformation in LCEs. This technique offers an accessible and reproducible method for fabricating aligned LCEs, which can be beneficial for early-stage research and educational purposes in soft material design and fabrication.

Received 18th November 2025,
Accepted 25th December 2025

DOI: 10.1039/d5ma01338k

rsc.li/materials-advances

1. Introduction

Liquid crystal elastomers (LCEs) represent a new generation of intelligent soft materials, distinguished by the directional ordering of liquid crystals and the reversible deformability of elastic polymer matrices.[1,2] Their unique ability to undergo reversible, large-scale deformations in response to external stimuli—such as heat, light, or electric fields—has positioned them as promising candidates for applications in soft robotics, artificial muscles, sensors, actuators, and tunable optics.[3] A critical factor influencing the performance of LCE-based devices is the orientation of the liquid crystal mesogens within the polymer network.[4] Proper alignment can lead to the formation of monodomain (aligned) LCEs, which exhibit uniform and enhanced mechanical or optical response compared to polydomain counterparts.[5–8] Achieving such alignment requires an effective alignment technique during the polymerization or cross-linking process. Several alignment strategies have been explored, including the use of magnetic[9–11] and electric fields,[12,13] photoalignment techniques,[14–17] shear flow,[18,19] and surface-induced alignment.[20–26] Among these, surface-induced alignment using rubbed polyimide films is particularly well-established. However, previous studies have relied on custom polyimide layers fabricated *via* spin coating or other deposition methods, which require cleanroom facilities, complex process flows, precise conditions, or specialized materials. These constraints limit the accessibility of such techniques for rapid prototyping, educational use, or low-cost fabrication. In this work, we present the first demonstration of surface-induced alignment of LCEs using commercially available Kapton HN films. These off-the-shelf substrates are widely accessible and do not require any chemical processing or coating steps. By mechanically rubbing the Kapton surface in a specific direction, we create a surface topology that induces mesogen alignment, resulting in the formation of monodomain

[a] *Department of Electrical Engineering, École de Technologie Supérieure (ETS), Montreal, QC H3C 1K3, Canada. E-mail: elaheh.asgari.1@ens.etsmtl.ca*
[b] *Department of Applied Sciences, Université du Québec à Chicoutimi (UQAC), Chicoutimi, QC G7H 2B1, Canada*
[c] *Microtechnologies Integration & Convergence Research Group, Université du Québec à Montréal (UQAM), Montreal, QC H2X 3Y7, Canada*

LCE films. This technique was tested using Kapton films rubbed either horizontally or vertically with respect to the film roll, enabling reproducible alignment conditions. The simplicity, low cost, and accessibility of this approach make it especially suitable for early-stage research and development, offering a convenient starting point for fabricating aligned LCEs.

2. Experimental

2.1 Sample preparation

RM1, RM2, and the photoinitiator (Irgacure® 651) were selected based on prior studies[27] and combined in an 12 : 87 : 1 weight ratio to form the LCE precursor mixture. The components were dissolved in ethanol and mechanically stirred at 100 °C for 20 minutes to ensure complete homogenization. The thermal properties of this composition were verified by differential scanning calorimetry (DSC), as shown in Fig. S1, which confirmed the glass transition temperature (T_g) and the nematic–isotropic transition temperature (T_{NI}) characteristics of the LCE system. Substrate preparation and film fabrication followed the process illustrated in Fig. 1. For planar-aligned K–H, K–N, and K–V configurations, 25 mm × 20 mm glass substrates and 15 mm × 10 mm Kapton HN films (12.7 μm thickness) were cleaned sequentially. First, the substrates and Kapton films were sonicated in acetone for 20 minutes, followed by sonication in isopropyl alcohol and rinsing with deionized water. The substrates were then dried using nitrogen, while the Kapton films were left to air dry. The Kapton films were fixed to glass substrates and unidirectionally rubbed using a homemade velvet-wrapped rubbing board for 10 minutes (30 back-and-forth strokes per min) per sample—along their length for K–H and along their width for K–V—to induce alignment. Isotropic LCE was prepared without the application of Kapton films. The LCE mixture was introduced by capillary action at 100 °C (isotropic phase) into cells formed by two glass substrates separated by a 25 μm spacer. Planar and twisted samples were photopolymerized under 365 nm UV light (OAI 800 MBA, mercury arc lamp, 17.5 A, 88 V) for 30 minutes in the nematic phase (55–65 °C), while isotropic samples were cross-linked under identical UV conditions at 100 °C. Upon curing, the LCE films were peeled from the substrates and cut into 8 mm × 1 mm strips aligned with the top-surface director for further characterization and thermal actuation measurements.

In total, seven LCE sample types were fabricated under three distinct cross-linking conditions: in the isotropic phase, in the nematic phase between two identically aligned planar substrates (planar alignment), and in the nematic phase between two planar substrates rotated 90° ssss relative to each other (twisted alignment).

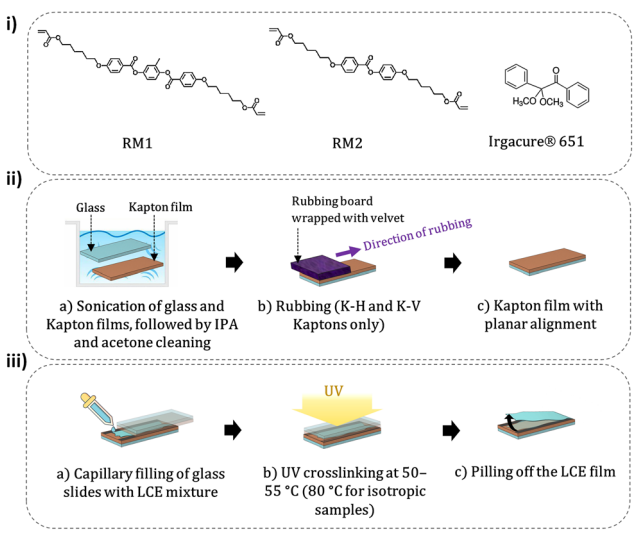

Fig. 1 Constituent structures and fabrication process of the LCE films. (i) Chemical structures of the LCE components: RM_1 and RM_2 as reactive mesogenic units, and Irgacure 651 as the photoinitiator. (ii) Schematic illustration of the planar alignment process for glass substrates. (iii) Fabrication steps for LCE films with different alignments (planar, twisted, and isotropic).

2.2 Measurement techniques

The thermal properties of the LCE composition were verified using DSC in a nitrogen atmosphere over a temperature range of −20 °C to 100 °C at a heating rate of 10 °C min^{-1}. The surface morphology and roughness of the Kapton films were analyzed using AFM (Bruker MultiMode 8). Top-view and cross-sectional images were obtained *via* POM (Keyence VHX-7000) operated in transmission mode to assess optical anisotropy and alignment quality. Thermal characterization was performed using a Nextron micro-probing station, offering precise temperature control in the range of 20 °C to 200 °C with a resolution of ±0.1 °C. The system enabled heating rates of up to 60 °C per minute and facilitated real-time video capture of the thermal response. Displacement of the sample was captured by a digital microscope camera (SKYBASIC) and analyzed with MATLAB image processing functions. Based on image resolution and pixel scaling, the measurement precision was within approximately 2%, ensuring reliable quantification of both in-plane and out-of-plane actuation. All LCE samples were fabricated under consistent processing conditions in an ISO Class 6 (Class 1000) cleanroom environment to ensure reproducibility and minimize contamination.

3. Results and discussion

3.1 Surface characterization of kapton

To investigate the effect of surface rubbing on Kapton films, three types of Kapton samples of identical dimensions (15 mm × 10 mm) were prepared. These were classified as follows: K–N, the unmodified Kapton film as received; K–H, Kapton rubbed horizontally along its length; and K–V, Kapton rubbed vertically, *i.e.* perpendicular to its length. Atomic force microscopy (AFM) measurements were conducted to evaluate the topography and roughness of each sample. The resulting AFM images for the Kapton films investigated are presented in Fig. 2.

Despite being exposed to no rubbing whatsoever, the K–N sample exhibits significant nanogrooves, originating from directional mechanical processing during film fabrication,

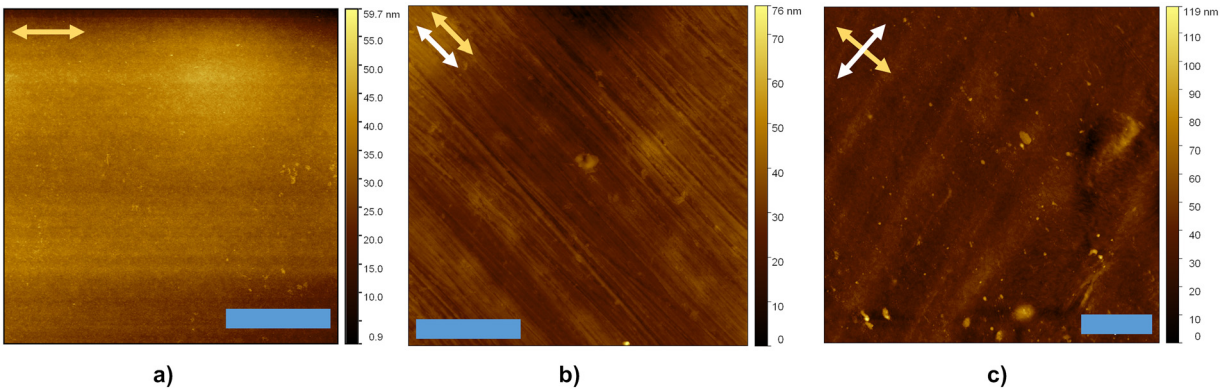

Fig. 2 AFM images of the three types of Kapton films analyzed: (a) K–N, (b) K–H, and (c) K–V. The yellow arrows show the direction of the pre-existing nanogrooves, while the white arrows indicate the direction of the applied rubbing. (Blue scale bars: 2 μm).

such as rolling. In the K–H sample, the rubbing direction is aligned with the length of the film which amplifies the existing grooves, resulting in a moderate increase in surface roughness.

In contrast, the K–V sample, which is rubbed perpendicularly to the original groove direction, exhibits the highest level of roughness. This can be attributed to the interaction between the new grooves and the pre-existing ones, leading to a more complex and irregular surface pattern. AFM topographies with profile trace lines used to measure groove depth and spacing, are provided in the supplementary information (SI) (Fig. S2 and Table S1). AFM characterization confirmed that rubbing direction significantly altered the surface morphology of Kapton substrates. As shown in Fig. S2, untreated Kapton (K–N) exhibited shallow pre-existing grooves, while parallel rubbing (K–H) produced deeper, more organized patterns, and perpendicular rubbing (K–V) introduced irregular features and intersecting scratches. These trends were quantitatively supported by the areal parameters summarized in Table S1, which demonstrate a systematic increase in roughness and surface complexity from K–N to K–H to K–V. Together, these results establish that rubbing direction governs nanogroove depth, periodicity, and overall topography, providing a controllable route for tuning alignment surfaces.

3.2 LCE alignment and morphology

Seven LCE sample variants are fabricated following the procedures detailed in the Experimental section. These samples are cross-linked under three alternate conditions: in the isotropic phase, in the nematic phase between two identically-aligned planar Kapton substrates (dubbed planar alignment), and in the nematic phase between two planar substrates rotated 90° relative to each other (dubbed twisted alignment). Accordingly, the samples are categorized in the following manner: planar-aligned ($LCE_{K-N\|K-N}$, $LCE_{K-H\|K-H}$, and $LCE_{K-V\|K-V}$), twisted-aligned ($LCE_{K-N\perp K-N}$, $LCE_{K-H\perp K-H}$, and $LCE_{K-V\perp K-V}$), as well as an isotropic sample (LCE_{iso}) serving as a control.

Amongst the planar-aligned LCEs, $LCE_{K-H\|K-H}$ exhibits the most uniform birefringent color under polarized optical microscopy (POM), indicating a highly aligned monodomain structure with mesogens oriented predominantly in one direction (Fig. 3c and j). $LCE_{K-N\|K-N}$ also demonstrates a high degree of alignment, suggesting that the pre-existing nanogrooves on the K–N substrate effectively guided the mesogen orientation (Fig. 3b and i). However, compared to $LCE_{K-H\|K-H}$, $LCE_{K-N\|K-N}$ exhibits minor polydomain regions due to the slightly less uniform surface texture of the Kapton. In contrast, $LCE_{K-V\|K-V}$ shows noticeable polydomain textures, as indicated by color variations in the POM images (Fig. 3d and k), which reflect poor mesogen alignment along a single direction.

In the twisted-aligned group, both $LCE_{K-N\perp K-N}$ and $LCE_{K-H\perp K-H}$ exhibit comparable birefringent textures with good uniformity, indicating successful twisted alignment. Cross-sectional POM is included to visualize the director variation through the film thickness, which cannot be captured from top-view images alone. This approach provides critical insight for comparative analysis of twisted LCE structures. As shown in Fig. 3l and m, the presence of two distinct birefringent colors (yellow and green) across the film's thickness confirms differential alignment between the top and bottom surfaces, consistent with a twisted configuration. Conversely, $LCE_{K-V\perp K-V}$ displays pronounced polydomain characteristics, especially in the cross-sectional POM view (Fig. 3n), where the presence of multiple colors suggests poorly defined director orientation along a single direction, resulting in inhomogeneous alignment.

3.3 Thermal actuation behavior

The thermal actuation behavior of monodomain LCEs, first reported by Küpfer and Finkelmann, originates from their intrinsic anisotropic molecular organization and the thermally induced transition between the nematic and isotropic phases.[28] In nematic LCEs, the mesogens are uniformly oriented along a defined direction, establishing a uniaxial nematic order characterized by the nematic director (**n**) and a scalar order parameter (Q).[29] Upon heating above the T_{NI}, thermal energy disturbs this alignment, leading to a significant reduction in the order parameter, where the contraction of aligned mesogens generates elastic strains and forces, while director rotation

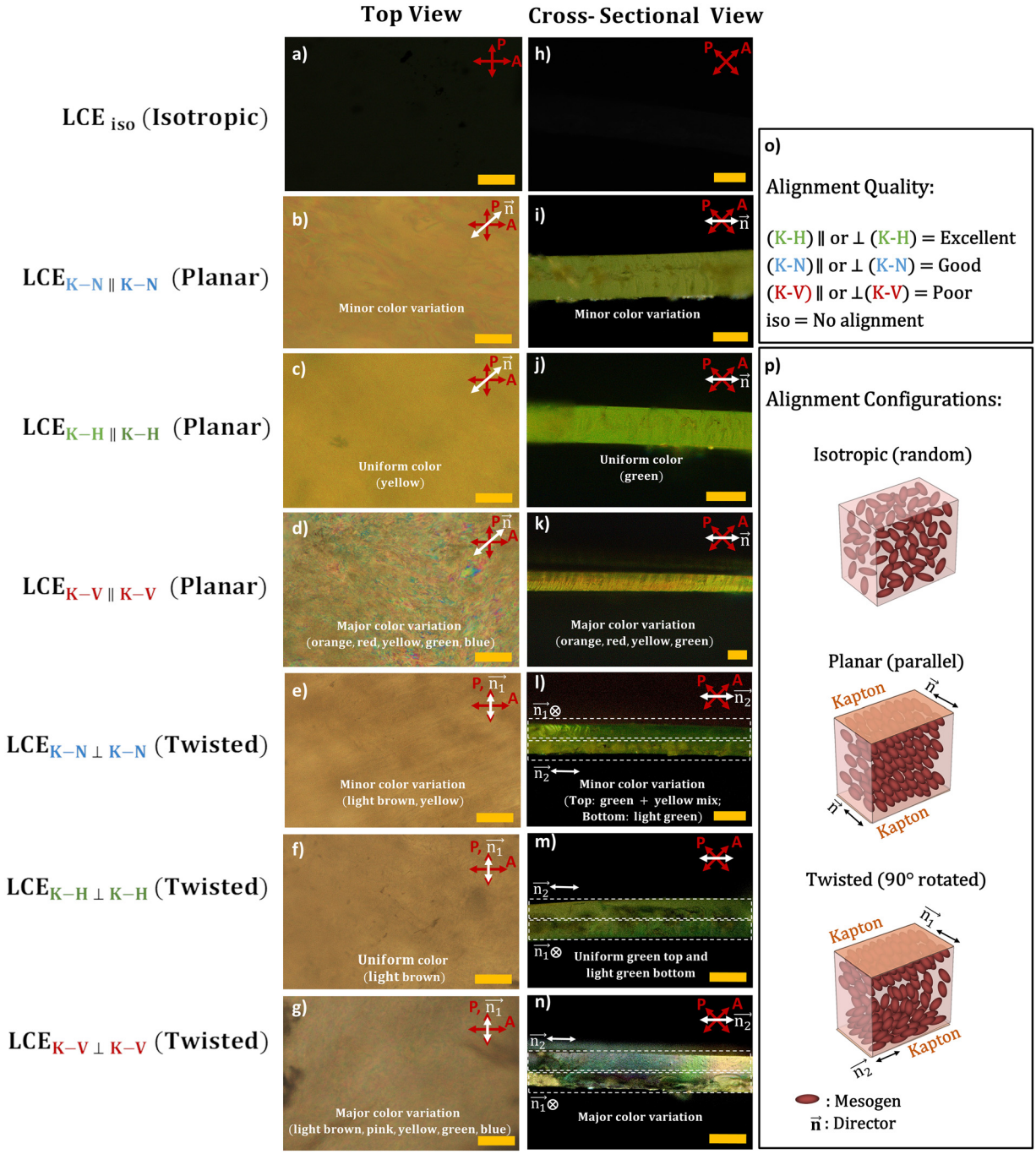

Fig. 3 Schematic illustrations and POM images of the fabricated LCE samples with distinct alignment configurations. The first column (a)–(g) presents top-view POM images of 25 μm thick LCE samples, while the second column (h)–(n) displays corresponding cross-sectional views, all captured under crossed polarizers in transmission mode. The samples include three planar-aligned LCEs ($LCE_{(K-N\|K-N)}$, $LCE_{(K-H\|K-H)}$, and $LCE_{(K-V\|K-V)}$), three twisted-aligned LCEs ($LCE_{(K-N\perp K-N)}$, $LCE_{(K-H\perp K-H)}$, and $LCE_{(K-V\perp K-V)}$), and one isotropic sample (LCE_{iso}). Red arrows indicate the orientation of the crossed polarizers, and white arrows denote the alignment direction of the LCE mesogens. For twisted-aligned LCEs, with distinct top and bottom directors ($\vec{n}_1$ and $\vec{n}_2$, respectively), cross-sectional POM images were acquired with polarizers at 45° to $\vec{n}_2$. Cross-sectional POM is included to visualize the director variation through the film thickness, which cannot be captured from top-view images alone. Panel (o) summarizes the alignment quality of LCEs fabricated using various Kapton substrates: K–H Kapton = excellent, K–N Kapton = good, K–V Kapton = poor, isotropic LCE = no alignment. Panel (p) shows schematic configurations of isotropic, planar-aligned, and twisted-aligned LCEs. (Scale bars: 25 μm).

induces torques and couple-stresses.[30] As a result, the elastomer undergoes a spontaneous contraction along the director axis due to the collapse of anisotropy within the polymer network.[30] This deformation is reversible: cooling the material below T_{NI} restores the nematic order, and the sample re-elongates along the original alignment direction.[31]

To investigate the influence of alignment configuration on thermal actuation behavior, all LCE samples were thermally stimulated from room temperature (25 °C) to 120 °C. Fig. 4 presents a schematic illustration of the thermal actuation mechanism corresponding to each alignment type, accompanied by representative snapshots of the LCE before and after actuation. For the planar-aligned LCEs (Fig. 4i), thermal actuation induced uniaxial contraction along the director axis. Among these, $LCE_{K-H\|K-H}$ and $LCE_{K-N\|K-N}$ exhibited the most pronounced contractions (27.56% and 11.50%, respectively), demonstrating effective alignment and order. In contrast, $LCE_{K-V\|K-V}$ showed only a minor contraction (1.18%), accompanied by multidirectional deformation (see Fig. 4i(g)), indicative of poor planar alignment and the presence of polydomain regions. The complex and limited actuation response observed in $LCE_{K-V\|K-V}$ is likely attributed to its non-uniform mesogen orientation.

For the twisted-aligned LCEs, two sets of thermal actuation tests were conducted to assess the directional bending behavior when the film was heated from either the bottom or top surface, referred to as "twisted (non-flipped)" and "flipped twisted" configurations, respectively. The key difference between these modes lies in the 90° rotation of alignment at the interface with the heating stage. In the non-flipped configuration (Fig. 4(ii)), thermal stimulation initiates a nematic-to-isotropic phase transition across the thickness of the LCE film.

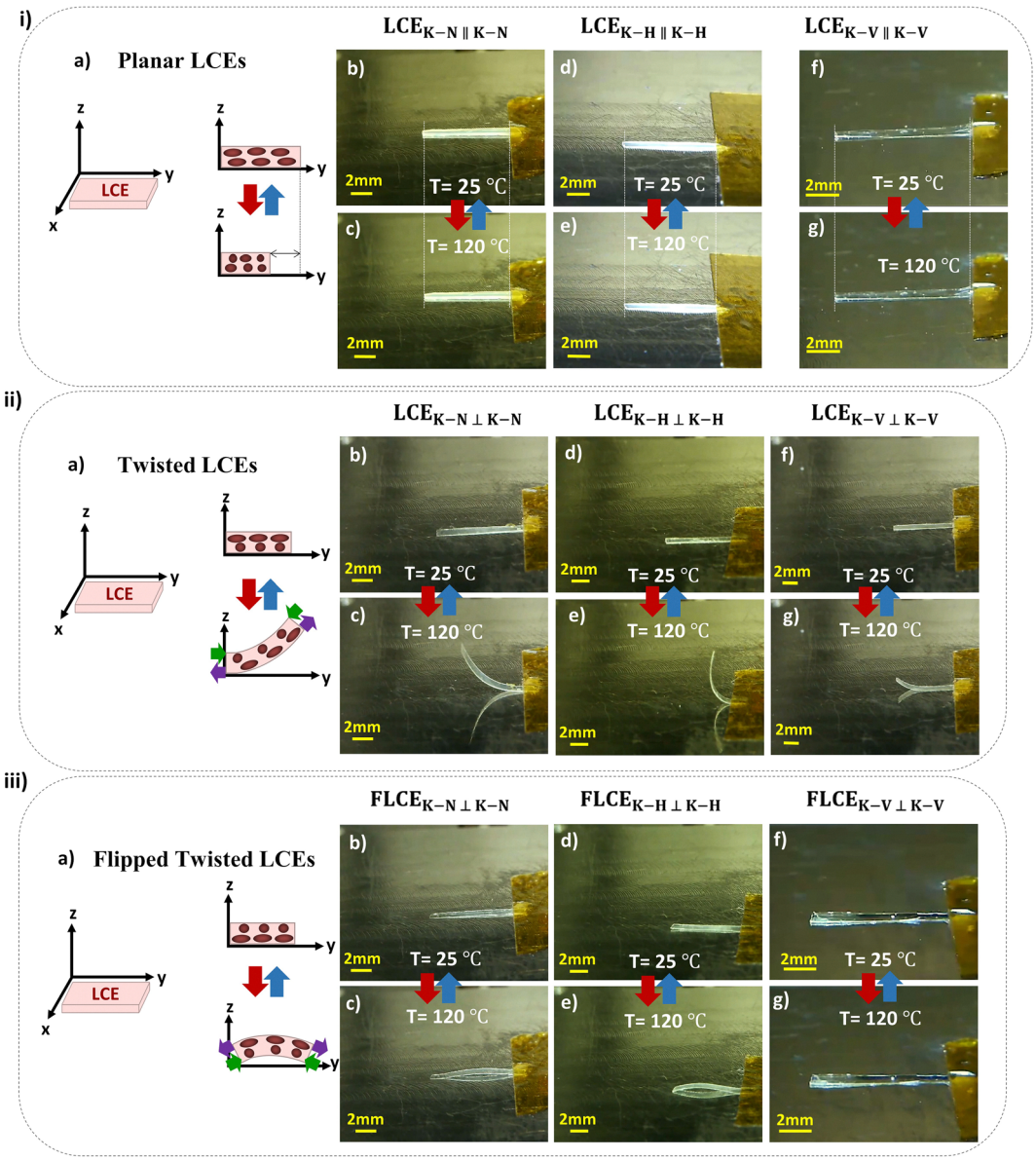

Fig. 4 Schematic illustration of the thermal actuation mechanism for each alignment configuration, accompanied by representative snapshots of the LCE samples before and after heating. Panel (a) in each group (i)–(iii) shows a schematic depiction of the thermal deformation behavior. The figure presents actuation of: (i) planar-aligned LCEs; (ii) twisted-aligned LCEs; and (iii) flipped twisted-aligned LCEs. All samples were subjected to thermal actuation by heating from room temperature (25 °C) to 120 °C.

Due to the twisted configuration of mesogen alignment between the top and bottom surfaces, the local director orientation varies continuously through the film's depth. As a result, each infinitesimal layer tends to contract uniaxially along its own director. However, because the preferred strain direction changes with depth, the film cannot deform uniformly and must instead accommodate the internal strain mismatch through bending. This phenomenon is illustrated in Fig. 4ii(a), which shows the deformation profile along the film's cross-sectional *YZ* plane. Upon heating, the top surface, with its mesogens aligned along one in-plane direction, undergoes contraction (green arrows), while the bottom surface, aligned in the orthogonal in-plane direction, undergoes relative expansion (purple arrows). The resulting asymmetric strain distribution through the thickness induces a curvature, manifesting as an upward bending of the LCE film. Simultaneously, for the flipped twisted LCE (Fig. 4(iii)), where the film is inverted such that the original bottom surface becomes the top surface, the opposite strain pattern emerges. As shown in the cross-sectional *YZ* view in Fig. 4iii(a), the new bottom surface (originally the top) now contracts, while the new top surface (originally the bottom) expands. This reversed asymmetry in strain induces a downward bending deformation, demonstrating the critical role of through-thickness director orientation in dictating the thermal actuation direction of twisted-aligned LCEs.

In both the twisted and flipped twisted configurations, $LCE_{K\text{–}H \perp K\text{–}H}$ demonstrated the most pronounced and consistent bending behavior, attributable to the high alignment quality at both surfaces, which ensures effective anisotropic deformation upon heating. In contrast, $LCE_{K\text{–}V \perp K\text{–}V}$ exhibited poor bending response in both configurations, consistent with its initial poor alignment quality and the presence of polydomain textures, which hinder coordinated actuation.

Additionally, the isotropic control sample, LCE_{iso}, which was crosslinked in the isotropic phase, displayed no appreciable motion due to the absence of any anisotropic ordering necessary for actuation. Fig. 5 presents the maximum deformation observed in the LCE films during heating from 25 °C to 120 °C. For twisted and flipped-twisted samples, the maximum out-of-plane deformation (Δz) is measured—specifically, the maximum tip displacement for twisted LCEs and the maximum dome-like bending height for flipped-twisted LCEs—while for planar-aligned samples, in-plane contraction (Δy) is recorded. Within each alignment group, LCEs fabricated with the K–H substrates exhibit the greatest displacement and a rapid response near the T_{NI} region, initiating actuation promptly. In contrast, LCEs prepared with the K–V substrates demonstrate the smallest displacement and a delayed actuation response.

To evaluate the effect of alignment configuration on the reversible shape transformation behavior, all LCE samples were subjected to a thermal cycle, wherein the temperature was increased from room temperature (25 °C) to 120 °C, and subsequently decreased back to 25 °C. The hysteresis curves illustrating the reversible thermal response of the LCE films are presented in Fig. 6. SI Video recordings documenting the actuation behavior are provided in the SI. As observed in all

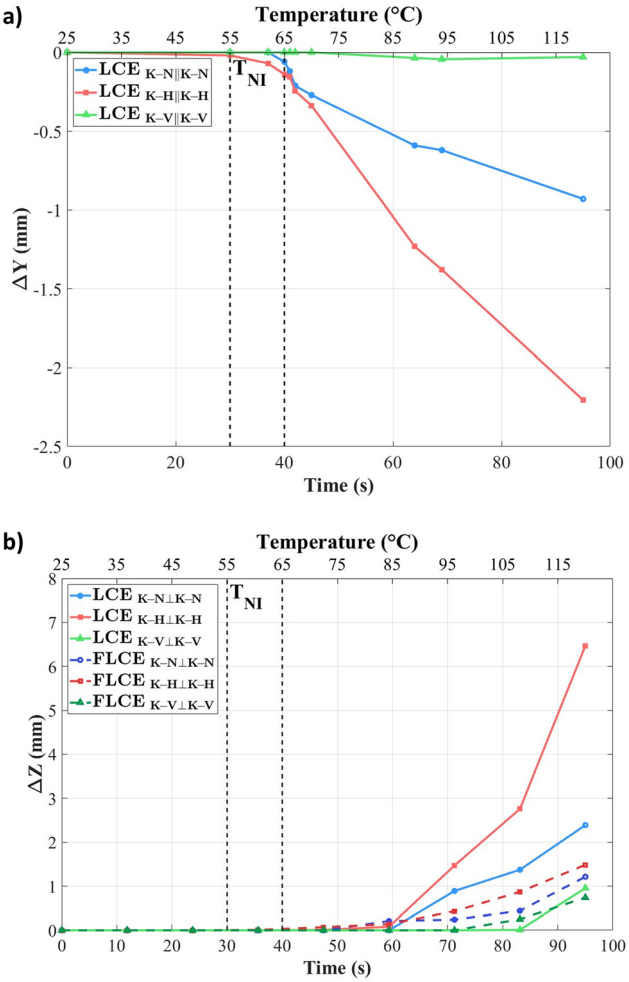

Fig. 5 Thermal displacement response of: (a) planar LCEs and (b) twisted LCEs and FLCE samples during heating from 25 °C to 120 °C. For twisted and flipped-twisted configurations, the maximum out-of-plane displacement (Δz) is plotted, while for planar configurations, in-plane displacement (Δy) is reported.

panels of Fig. 6, the onset temperature of actuation is strongly dependent on alignment quality. Well-aligned LCE samples fabricated using K–H substrates begin to deform at lower temperatures (often near 55–65 °C), consistent with efficient nematic ordering and early phase transition. Conversely, LCE samples with poor alignment, such as those prepared with K–V substrates, require substantially higher temperatures to initiate actuation, often well above the nominal T_{NI}. This delay is due to the energy required to overcome internal frustration and enable mesogen reorientation across misaligned domains. These results confirm that alignment quality not only controls the amplitude and direction of actuation but also determines the speed, reversibility, and thermal onset of the response.

3.4 Discussion

This study systematically investigated the thermal actuation behavior of monodomain LCEs fabricated using a surface-induced alignment method based on mechanically rubbed

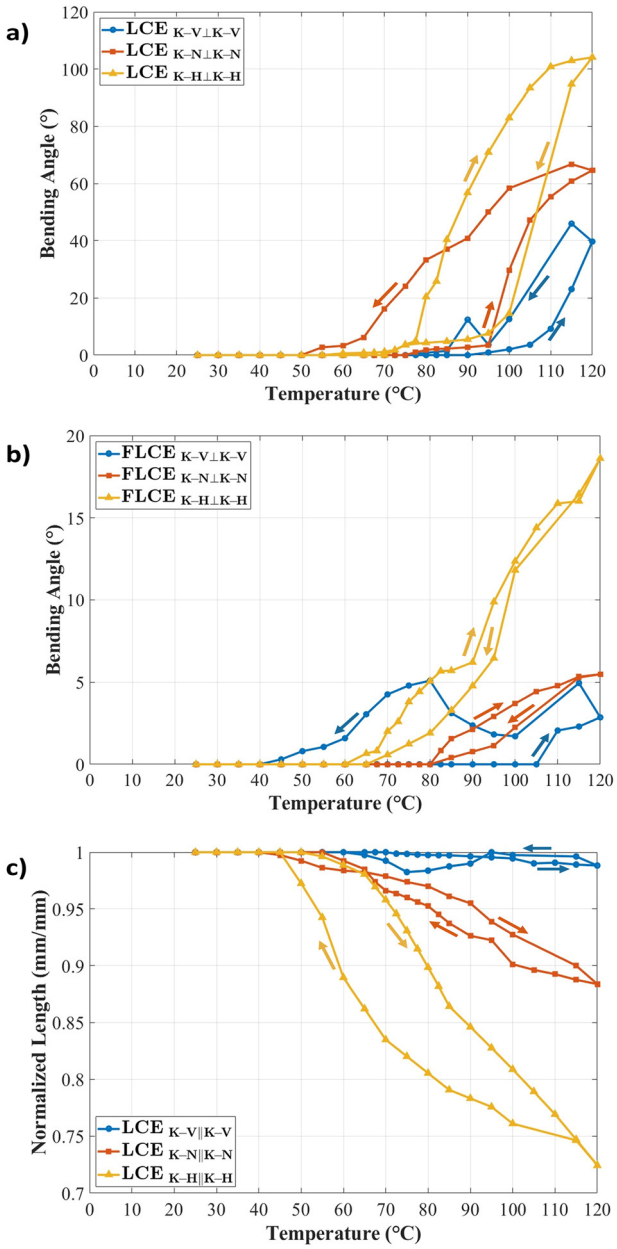

Fig. 6 Thermal hysteresis behavior of LCE films with different alignment configurations and substrate-induced alignment qualities: (a) twisted aligned LCEs, (b) flipped twisted aligned LCEs, and (c) planar aligned LCEs. Graphs (a) and (b) display the bending angle measured relative to the surface of the hot stage, while graph (c) shows the normalized length during contraction and expansion, all plotted as a function of temperature during a heating cycle from 25 °C to 120 °C and subsequent cooling back to 25 °C.

commercial Kapton films. The experimental results highlight the critical role of alignment configuration, mesogen orientation, and surface topography in governing the directionality and magnitude of LCE deformation in response to thermal stimuli.

Among all tested configurations, the $LCE_{K–H\perp K–H}$ demonstrated the largest out-of-plane displacement upon heating. This pronounced bending behavior is attributed to the high alignment fidelity achieved on both film surfaces, due to the dense and unidirectional nanogrooves produced by rubbing. The strong strain gradient across the film thickness, caused by opposing thermal responses on each surface, resulted in anisotropic bending. This configuration is particularly effective for flexural actuation applications, including soft grippers, artificial muscles, and bioinspired bending structures.

LCEs made with K–N Kapton (like $LCE_{K–N\perp K–N}$) also showed considerable bending displacement, though slightly lower in magnitude compared to their K–H counterparts. The performance of these samples is attributed to the unidirectional but finer nanogroove structures on the K–N surfaces, which supported reasonably good mesogen alignment. Importantly, K–N-based LCEs offer a more accessible and reproducible processing route, as the K–N Kapton enables alignment without the need for any surface rubbing, thereby minimizing alignment defects and simplifying fabrication. Therefore, K–N-based LCEs present a practical alternative for scenarios where moderate actuation with simpler fabrication is desired. In contrast, LCEs fabricated using K–V kapton, either in planar or twisted configurations, consistently exhibited poor actuation performance. The intersecting nanogroove patterns observed on K–V surfaces led to disordered or multidomain mesogen orientation, which limited coordinated deformation during thermal cycling. These findings underscore the importance of avoiding K–V configurations when directional or predictable actuation is required. Planar-aligned samples, particularly $LCE_{K–H\parallel K–H}$ and $LCE_{K–N\parallel K–N}$, demonstrated uniaxial in-plane contraction upon heating, consistent with monodomain behavior. While these planar samples did not produce out-of-plane motion, they are well-suited for applications such as linear actuators or strain-responsive films. Notably, the consistent in-plane response further validates the quality of alignment achieved through surface rubbing, especially with K–H substrates. Although all samples exhibited actuation onset near the T_{NI}, typically between 55 °C and 65 °C, the nature of the actuation response varied significantly depending on the alignment quality. In well aligned LCEs (like $LCE_{K–H\perp K–H}$, Fig. 5b), the mesogens are uniformly aligned along a single director, allowing the nematic-to-isotropic transition to proceed coherently upon heating. Although local constraints exist due to the polymer network and finite chain mobility, these constraints are directionally consistent and support a smooth and gradual reduction in the Q beginning near the nominal T_{NI}. As a result, actuation occurs progressively with increasing temperature. In addition, as reported by Rogóż *et al.*,[7] better-aligned LCEs exhibit lower storage modulus along the alignment direction—reflecting mechanical softness that facilitates mesogen reorientation. This lower stiffness supports the cooperative deformation of the network, contributing to a continuous and responsive actuation behavior close to T_{NI}. In contrast, slightly polydomain LCEs (like $LCE_{K–V\perp K–V}$, Fig. 5b), exhibit locally varying director orientations and competing deformation modes. These internal mismatches generate heterogeneous elastic constraints that suppress uniform mesogen reorientation at lower temperatures. As thermal energy accumulates, the scalar order parameter begins to decrease locally, but mechanical frustration between domains resists macroscopic deformation. Once

sufficient thermal energy is supplied—often well above T_{NI}—a critical threshold is reached where the nematic order collapses across a significant portion of the sample. This sudden breakdown releases the accumulated internal strain, allowing the polymer network to deform more freely. The result is a delayed yet pronounced actuation response, reflecting the collective relaxation of frustrated domains into a lower-energy isotropic configuration. As shown in Fig. 5, the alignment configuration not only affects the magnitude of deformation but also governs the mode and dynamics of actuation, particularly through its influence on mesogen reordering pathways and strain propagation. The hysteretic behavior observed in the LCE samples, as depicted in Fig. 6, is strongly correlated with the alignment quality achieved using different Kapton substrates. Clockwise hysteresis, consistently seen in LCEs fabricated with K–H substrates, indicates energy dissipation during actuation and recovery. These well-aligned films exhibit rapid, coordinated mesogen reorientation, enabling smooth deformation and relaxation near the T_{NI}. To validate the direction of hysteresis in thermally actuated planar LCEs, Lee *et al.* reported a similar clockwise hysteresis trend in planar LCEs synthesized using three different isomeric amines for chain extension.[32] In contrast, counterclockwise hysteresis, observed in some LCEs made with K–N and K–V substrates, reflects the accumulation and delayed release of internal strain energy. This behavior is attributed to the presence of slightly polydomain regions, where local director misalignments and mechanical frustration hinder immediate mesogen relaxation. Upon reaching a critical temperature threshold, these frustrated domains undergo a sudden cooperative transition, releasing stored energy and producing a sharp actuation response. LCEs fabricated with K–N substrates exhibit intermediate hysteresis behavior, reflecting their moderate alignment quality and partial mesogen cooperativity. Meanwhile, K–V-based LCEs, with the poorest alignment, initiate actuation well above T_{NI} and display sluggish, irregular responses, further emphasizing the role of alignment quality in governing both the onset and dynamics of hysteresis. Taken together, these results offer practical guidance for selecting alignment configurations based on target performance. For maximum bending displacement and sensitivity, twisted $LCE_{K–H\perp K–H}$ are recommended. For easier processing with acceptable actuation, twisted $LCE_{K–N\perp K–N}$ configurations provide a strong balance between performance and fabrication simplicity. $LCEs_{K–H\parallel K–H}$ or $LCEs_{K–N\parallel K–N}$ can be used when directional in-plane contraction is desired, while configurations involving K–V Kapton should be avoided due to unreliable alignment and minimal actuation. These findings reinforce the importance of optimizing surface nanostructure for LCE fabrication and provide a foundation for future design strategies in soft actuator and sensor technologies.

4. Conclusions

This study marks a pivotal shift from the conventional approach of liquid crystal alignment on rubbed polyimide coatings. We demonstrate, for the first time, that off-the-shelf Kapton HN films—without any chemical treatment or spin-coating—can function as robust alignment substrates for LCEs. Unlike prior methods that relied on custom-fabricated polyimide layers, which introduce complexity, cost, and variability, our strategy removes these constraints entirely. By leveraging commercially available materials and a straightforward rubbing process, we provide a reproducible, low-cost alignment technique that significantly broadens accessibility. This advancement enables streamlined fabrication of responsive soft materials, making LCE technology more practical for research, prototyping, and educational applications.

By tailoring the rubbing direction on Kapton HN substrates, we systematically investigated the influence of surface-induced nanogroove patterns on the alignment quality of LCEs and their corresponding thermal actuation behavior. AFM characterization revealed that rubbing in different directions generated distinct surface roughness profiles, which directly impacted the alignment of mesogenic units within the polymer matrix. POM analysis confirmed that K–H substrates produced the most uniform and monodomain alignment, resulting in superior actuation performance. The thermal response of LCEs was strongly influenced by alignment quality, not only in amplitude and direction but also in onset temperature and hysteresis behavior. Well-aligned K–H samples exhibited early actuation near 55–65 °C and showed clockwise hysteresis, indicating efficient energy dissipation and rapid mesogen reorientation. In contrast, poorly aligned K–V samples displayed delayed, irregular actuation and counterclockwise hysteresis, reflecting internal strain buildup and frustrated domain transitions. K–N-based LCEs showed intermediate behavior, balancing performance and ease of fabrication. Alignment quality was assessed through an integrated approach combining AFM surface characterization, POM imaging (top-view and cross-sectional), and thermal actuation measurements, including hysteresis analysis. Unlike previous studies that primarily quantified alignment through structural metrics, this work introduced a functional evaluation strategy by correlating surface morphology with actuation performance. The consistency among these methods confirms that rubbing direction governs nanogroove morphology, which in turn dictates mesogen orientation and actuation behavior.

Our findings establish a direct correlation between Kapton-induced surface features and the functional behavior of LCEs, offering valuable insights for the rational design of responsive soft materials. This accessible alignment strategy holds promise for broad implementation in research settings, particularly for the prototyping of soft actuators, sensors, and educational demonstrations in the field of smart materials.

Conflicts of interest

There are no conflicts to declare.

Data availability

The data supporting the findings of this study are available within this article and its supplementary information (SI).

Supplementary information is available. See DOI: https://doi.org/10.1039/d5ma01338k.

Acknowledgements

This work was financially supported by the Regroupement Stratégique en Microsystémes du Québec (ReSMiQ) and the Natural Sciences and Engineering Research Council of Canada (NSERC), with infrastructure and technical assistance provided by the Laboratoire de communications et d'intégration de la microélectronique (LACIME). The authors also thank the Nano-QAM laboratory at UQAM for providing access to advanced characterization facilities and for their invaluable assistance throughout the experimental phase of this study.

Notes and references

1 J. Sun, W. Chao, L. Yongjiao, L. Xudong and Z. Wang, *Int. J. Smart Nano Mater.*, 2023, **14**, 440–459.
2 J. M. Boothby, H. Kim and T. H. Ware, *Sens. Actuators, B*, 2017, **240**, 511–518.
3 E. Asgari, A. Robichaud, P.-V. Cicek and A. Shih, *J. Mater. Chem. C*, 2024, **12**, 15359–15381.
4 M. Cheng, Z. Wang, Z. Wu, S. Yuan, M. Cen, J. Wang and Y. J. Liu, *Macromo. Rapid Commun.*, 2025, **46**(14), 2500001.
5 K. M. Herbert, H. E. Fowler, J. M. McCracken, K. R. Schlafmann, J. A. Koch and T. J. White, *Nat. Rev. Mater.*, 2022, **7**, 23–38.
6 J. Zhao, L. Zhang and J. Hu, *Adv. Intell. Syst.*, 2022, **4**, 2100065.
7 C. P. M. Linares, N. A. Traugutt, M. O. Saed, A. M. Linares, C. M. Yakacki and T. D. Nguyen, *Soft Matter*, 2020, **16**, 8782–8798.
8 M. Kondo, Y. Yu and T. Ikeda, *Angew. Chem., Int. Ed.*, 2006, **45**, 1378–1382.
9 M. I. Boamfa, S. V. Lazarenko, E. C. M. Vermolen, A. Kirilyuk and T. Rasing, *Adv. Mater.*, 2005, **17**, 610–614.
10 S. Li, M. Aizenberg, M. M. Lerch and J. Aizenberg, *Acc. Mater. Res.*, 2023, **4**, 1008–1019.
11 H. Zeng, O. M. Wani, P. Wasylczyk, R. Kaczmarek and A. Priimagi, *Adv. Mater.*, 2017, **29**, 1701814.
12 A. Münchinger, V. Hahn, D. Beutel, S. Woska, J. Monti, C. Rockstuhl, E. Blasco and M. Wegener, *Adv. Mater. Technol.*, 2022, **7**, 2100944.
13 W. H. D. Jeu, *Liquid Crystal Elastomers: Materials and Applications*, Springer, 2012.
14 M. Gao, M. Cheng, W. Cai, Y. Liu, H. Dai and Y. J. Liu, *Optics Lasers Eng.*, 2024, **179**, 108254.
15 X. Pang, J.-a Lv, C. Zhu, L. Qin and Y. Yu, *Adv. Mater.*, 2019, **31**, 1904224.
16 B. A. Kowalski, V. P. Tondiglia, T. Guin and T. J. White, *Soft Matter*, 2017, **13**, 4335–4340.
17 Y. Folwill, Z. Zeitouny, J. Lall and H. Zappe, *Liq. Cryst.*, 2021, **48**, 862–872.
18 W. Helfrich, *J. Chem. Phys.*, 1969, **50**, 100–106.
19 S. Umerova, D. Kuscer, M. Bobnar, N. Derets, B. Zalar and A. Rešetic, *Mater. Des.*, 2021, **207**, 109836.
20 Y. Xia, G. Cedillo-Servin, R. D. Kamien and S. Yang, *Adv. Mater.*, 2016, **28**, 9637–9643.
21 A. Rešetic, *Commun. Chem.*, 2024, **7**, 1–14.
22 Z. Wang, T. Raistrick, A. Street, M. Reynolds, Y. Liu and H. F. Gleeson, *Materials*, 2023, **16**, 393.
23 Y. Wang, A. Dang, Z. Zhang, R. Yin, Y. Gao, L. Feng and S. Yang, *Adv. Mater.*, 2020, **32**, 2004270.
24 J. Wang, K. Li, H. He, W. Cai, J. Liu, Z. Yin, Q. Mu, V. K. S. Hisao, D. Gérard, D. Luo, G. Li and Y. J. Liu, *Laser Photonics Rev.*, 2022, **16**, 2100396.
25 M. Gao, J. Wang, W. Cai, M. Cheng, X. Hao, Y. Wang, Y. Liu, D. Kong, J. Liu, H. Dai and Y. J. Liu, *Nanophotonics*, 2023, **12**, 4205–4214.
26 H. He, J. Wang, K. Li, M. Cen, W. Cai, J. Liu, D. Luo, Y.-Q. Lu and Y. J. Liu, *Laser Photonics Rev.*, 2022, **16**, 2200115.
27 C. Feng, C. P. H. Rajapaksha, J. M. Cedillo, C. Piedrahita, J. Cao, V. Kaphle, B. Lüssem, T. Kyu and A. Jákli, *Macromol. Rapid Commun.*, 2019, **40**, 1900299.
28 J. Küupfer and H. Finkelmann, *Macromol. Chem. Phys.*, 1994, **195**, 1353–1367.
29 M. Warner, K. P. Gelling and T. A. Vilgis, *J. Chem. Phys.*, 1988, **88**, 4008–4013.
30 H. Jiang, C. Li and X. Huang, *Nanoscale*, 2013, **5**, 5225–5240.
31 X. Tian, Y. Guo, J. Zhang, O. M. Ivasishin, J. Jia and J. Yan, *Small*, 2024, **20**, 2306952.
32 Y. Lee, S. Choi, B.-G. Kang and S.-K. Ahn, *Materials*, 2020, **13**, 3094.